Introduction

Laser-induced periodic surface structures were detected in early experiments on laser application [Bir65] and have been studied experimentally ever since. The first widely accepted theoretical approach [EHW73], [SYP83] describing LIPSS suggested that the structures are the result of an interference of the incoming laser beam with some form of a surface-scattered electromagnetic wave traveling along the surface. The interference theory accounted well for a dependence of the ripples' orientation on the laser polarization. Also the cumulative effect of the laser irradiation has been taken into account by this model [YPD83], [YSD84]. In general, this theory was successful in the description of uniformly distributed patterns with the periodicity dependent on the laser wavelength and on the angle of incidence [Bir65], [SKK73], [EHW73], [YPD83], [YSD84], [BoH03] observed under long-pulse (ns) irradiation.

The application of femtosecond laser pulses, however, has revealed a large, much more complex diversity of patterns at the modified surface region. Such micro- and nanostructured areas exhibit surprising novel optical and mechanical properties, which offer a great potential application in various modern technologies. For instance, direct laser writing [KST01], special wettability (so-called "lotus-effect") [GrM06], [ZPP06], controllable reflectance of metals [VoG08], color marking [DSS09], as well as producing of "black silicon" [SKI08] are based on the ability of femtosecond laser to precise non-thermal material modifications.

Arrays of periodic linear structures with many bifurcations and with periods substantially shorter than the applied laser wavelength were reported in numerous publications of the end the 90s and beginning of the 2000s, some of them cited here [VWR98], [BSS00], [CHR02], [SKS05]. Their orientation and shape were generally dictated by polarization of the incident laser beam [RCH02], [CKR04], [MiM07], [DRD09], [BRK09]. Numerous experimental data have shown that usually the ripples completely develop only after a considerable number of pulses [BSS00], [BBK02], [BBM04], [CHR02], [CHR03], [BoK10], and that positive feedback plays an important role in the structure formation process [Rei09], [BoK10]. These peculiar features of "femtosecond ripples" do not comply with the "classical ripples theory" based on a locally modulated energy input due to the interference effect [EHW73], [SYP83], [YPD83], [YSD84]. The ripples exhibit non-trivial surface morphology, sharing many similarities with other self-organized patterns originating from instabilities [MiV03], [TBL98], [EAC99]. The periodicity seems to be insensible to the laser wavelength and incident angle, but it is correlated with the local intensity of

the laser beam [CHR02], [KRD05]. Formation mechanisms of laser-generated ripples and the underlying microscopic processes are still discussed.

Several years ago, taking into account all these facts and the strong nonequilibrium conditions of femtosecond laser ablation, self-organized pattern formation from the laser-induced surface instability was proposed by J. Reif and M. Bestehorn [HVW99], [CHR02], [RCB06] as a possible scenario for femtosecond ripples.

A systematic study on the surface nanostructuring upon femtosecond laser ablation is presented in this work. The various experimental parameters that control surface morphologies are investigated. The effect of laser polarization, an irradiation dose, surface defects and an important role of a multipulse feedback in structure formation are analyzed, based on a statistical evaluation of numerous experimental data. To gain more information about possible microscopic mechanisms of the ripples' formation, the thorough surface investigation of structured samples was also supplemented by a cross-sectional analysis and electrical measurements.

The dissertation is organized as follows:

The first chapter considers the fundamental mechanisms of the ultra-short pulsed laser-matter interaction that is characterized by a nonequilibrium nature of the processes. For various target materials, different microscopic mechanisms for absorption and dissipation of the laser energy, resulting in the macroscopic material removal/ablation, are discussed.

Results of the experimental and theoretical studies on laser-induced periodic surface structures are briefly reviewed in the second chapter. Here, special attention is paid to the peculiar features of the femtosecond LIPSS that cannot be explained by a widely accepted classical approach attributing ripple formation to an inhomogeneous energy deposition due to optical interference. Based on the critical analysis of existing theoretical studies, surface self-organization from laser-induced instability is proposed as the possible origin mechanism for femtosecond nanostructuring. According to this approach, femtosecond nanostructures arise from laser-induced surface erosion counterbalanced by thermal self-diffusion.

In the third chapter, an adopted surface erosion model for pattern formation upon femtosecond pulsed laser ablation is introduced. The dependence of generated patterns on the incident laser electric field is taken into account. The approach is based on the description of surface pattering by an energetic ion beam. The surface morphologies obtained in the framework of this model for different polarization directions and time periods are in excellent agreement with experimental results.

Representation of the experimental results of the dissertation begins with the fourth chapter. At the beginning, the brief review of technique and procedure of laser ablation experiments and the subsequent investigation of the structured samples is given.

Experimental studies of the parameters controlling the self-organized pattern formation process are presented in the fifth chapter. Laser polarization and the incidence angle of the laser beam, irradiation dose and surface defects, as well as a multipulse feedback effect are the focus of this chapter.

The sixth chapter is devoted to the in-depth investigations of the laser-modified silicon. The intrinsic modifications of the irradiated material, which indicate a very fast non-thermal surface relaxation from a highly nonequilibrium state, give strong support to the conception of self-organization from laser-induced instability as the origin of ripples.

General conclusions and outlook are given in the last chapter. Ripples generated on different target materials are compared. Control parameters common for dielectrics, semiconductors and metals as well as the similarity in shape and the size of the laser-induced morphologies confirm a universal mechanism of structuring, which is consistent with self-organization.

1. Laser ablation and laser-induced surface instability

1.1. General aspects of pulsed laser ablation

Laser ablation denotes, by definition, the removal of macroscopic amounts of matter from the surface of condensed matter upon intense − usually pulsed − laser irradiation. It is, commonly, characterized by a threshold fluence below which only desorption of individual particles is observed, without any noticeable surface modification. Since the laser is coupled to the target's electronic system, the ablation yield strictly depends on the electronic excitation density [Mil94] but follow-up processes such as excitation dissipation, thermal material response (melting, evaporation) and other material removal processes (direct electronic bond breaking [Bae96], [Sri86], phase explosion [MiK95], Coulomb explosion [Rei89], [HWR00], [SRA02] play an important role. In a general scheme (Fig. 1.1), the complex process chain from laser impact to ablation can be summarized [Bae96].

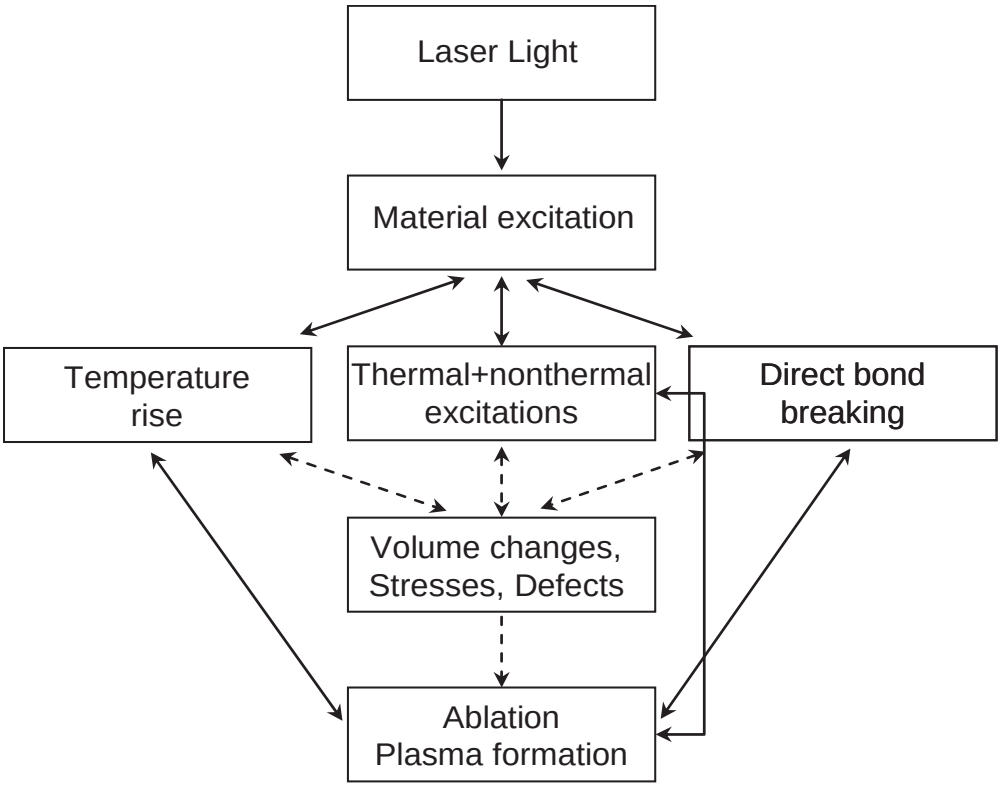

Fig. 1.1: Laser-matter interaction and feedback mechanisms during ablation. Different scenarios are possible: thermally activated ablation (left path), non-thermal photochemical ablation (right), and a combination of both (at the middle), (after [Bae96]).

After the material excitation by the incident laser pulse, one can distinguish, in principle, three main scenarios: (1) the deposited energy is completely transferred into

heat, (2) the absorbed laser light results in direct photochemical bond breaking, or (3) a combination of non-thermal bond breaking and thermal excitation is induced. All three dissipation channels can lead to direct material removal, e.g. by expulsion or melting/evaporation, respectively sublimation. Another possibility is an indirect process where, in an intermediate step, the material is first modified and only subsequent pulses remove this modified material. Both material removal and material modification can influence, in turn, the optical, thermal, and mechanical material properties and thus have a positive or negative feedback on subsequent excitation, dissipation and ablation processes.

This chapter will be mainly addressed to the fundamental mechanisms of interaction of an ultrashort pulsed laser irradiation of different targets (dielectric, semiconducting and metallic). When such short pulses (duration about 100 fs) are involved, additional particular features, such as temporal separation of laser excitation and massive particles emission, have to be considered in the ablation dynamics.

1.2. Electronic excitation

Laser ablation of materials starts with energy deposition in the electronic subsystem of a target through linear and non-linear absorption that leads to a high density of hot electrons in the conduction band. While in nonmetallic targets the free electron density increases during the pulse due to intraband transitions, in metals the density hardly changes, but the kinetic energy of free electrons drastically grows. A detailed picture of these effects will be presented in the next paragraphs.

1.2.1. Nonlinear absorption/ionization in *dielectrics*

When an intensive laser beam with photon energy less than the band gap of the material ($\hbar\omega << E_{gap}$) impinges on the surface of a transparent target, absorption and free electron generation in the conduction band can occur only through nonlinear processes such as multiphoton- or impact ionization [Kel65], [SKB77], [Rei89], [Blo74], [RSL04].

A first theoretical analysis of ionization of atoms in a strong light field was performed by Keldysh [Kel65]. He obtained the general equation for the photoionization probability, where, depending on the laser frequency and laser intensity, multiphoton and tunneling ionization can be considered as two limiting cases of the general solution. According to this theory [Kel65], the ionization probability for different processes is given by the parameter γ that is determined as the ratio between the frequency of laser light, ω, and the frequency ω_t of electrons tunneling through a potential barrier:

$$\gamma = \frac{\omega}{\omega_t} = \frac{\omega\sqrt{2m^*\varepsilon_i}}{eE}, \tag{1.1}$$

where E describes the laser electric field; ε_i denotes ionization energy of an atom; e is electron charge and $m^* = \frac{m_C m_V}{m_C + m_V}$ is the electron's reduced effective mass, with m_C and m_V the effective mass of the electrons in the conduction and valence band, respectively.

From Keldysh's approach [Kel65] it follows that at high laser frequencies ($\gamma >> 0$), multiphoton ionization (MPI) is the dominant mechanism of free electron generation. The probability P of MPI is correlated with the laser intensity I by the power law [Del75]:

$$P = \sigma^{(n)}(I) I^n, \tag{1.2}$$

where index n is the order of the multiphoton process, which shows how many photons will be absorbed by an electron in one elementary excitation act; and $\sigma^{(n)}(I)$ is the macroscopic absorption cross section that depends on the laser intensity for a strong incident laser field [Rei09].

The electron transition into a free state is accomplished by simultaneous absorption of n photons (process I in Fig. 1.3 (a)), in which total energy E_{abs} should be equal or exceed the band-gap energy and is given by [Rei89], [BeG66]:

$$E_{abs} = \sigma^{(n)} I^n \tau_{pulse} = \sigma^{(n)} I^{n-1} F, \tag{1.3}$$

where F is the laser fluence and τ_{pulse} is the laser pulse duration. The process can additionally be enhanced by localized defect states within the band gap (process II in Fig. 1.3 (a)). The resultant number of extracted electrons, or electron yield Y_{el}, is also proportional to the laser intensity I and follows the power low [Rei89], [BeG66]:

$$Y_{el} \propto I^n. \tag{1.4}$$

Indeed, the power law dependence of the electron yield Y_{el} on the laser intensity I (1.4) is in good agreement with data of time-of-flight mass spectra taken upon ablation of different wide band gap dielectrics [RCE04], [Cos07]. The slopes of the linear functions in Fig. 1.2 indicate a nonlinear ionization process, but the nonlinearity may

be less than expected from the band gap. The phenomenon can be explained by laser induced localized or transient defect states within the band gap [Rei89]. As shown in the insert in the Al_2O_3 panel (Fig. 1.2), localized energy states within the band gap, e.g. due to formation of an F-center (an anion vacancy), may act as intermediate resonances and reduce the order of nonlinearity [Rei09].

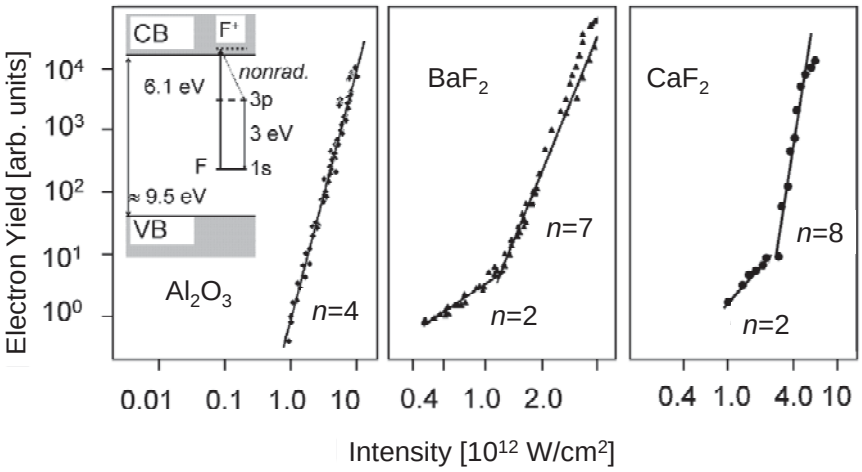

Fig. 1.2: Double logarithmic plot of electron yield as a function of laser intensity after irradiation with laser pulses at photon energy 1.55 eV of three different dielectric targets: Al_2O_3 ($E_{gap} \approx 9.5$ eV [ArW68]), BaF_2 ($E_{gap} \approx 10.5$ eV [KKR87]), and CaF_2 ($E_{gap} \approx 12$ eV [Rub71]). The slopes of the linear functions suggest *n*-photon absorption. The insert in the Al_2O_3 panel shows, schematically, the band-structure (VB: valence band and CB: conduction band) and the energy levels of a localized F-center with a 1s ground state, a 3p excited state, and the ionized F^+-center energy in the conduction band. (after [Rei09])

In the other limiting case $\gamma \ll 1$, corresponding to low irradiation frequencies or very strong laser fields (E ~ 200 MV/cm), tunneling of an atomic electron through a potential barrier under the action of an external electric field is reported to be main scenario for free electron generation [Kel65]. Here the ionization probability P depends exponentially on the laser electric field E [Del75]:

$$P = \frac{b}{\sqrt{E}} \exp\left(-\frac{c}{E}\right), \tag{1.5}$$

where b and c are constants and the exponential has a well known expression for the tunnel auto-ionization of atoms in a constant electric field [LaLd87].

In contrast to multiphoton and tunneling ionization, where the transition of electrons from the valence band to the conduction band is assisted by the laser electric field, Auger-like impact ionization is caused by already existing free electrons in the

conduction band. Those can be provided, for instance, by ionized defect states [Cos07] or by photoionization [Kel65]. As shown in Fig. 1.3 (b), the conduction band electrons gain additional energy in the laser field via inverse Bremsstrahlung (step I). If its kinetic energy is sufficiently large, part of this energy can be transferred in an Auger-like process to a valence band electron (step II), thus exciting it to the conduction band (step III) [Blo74]. The impact ionization may even result to an electron avalanche.

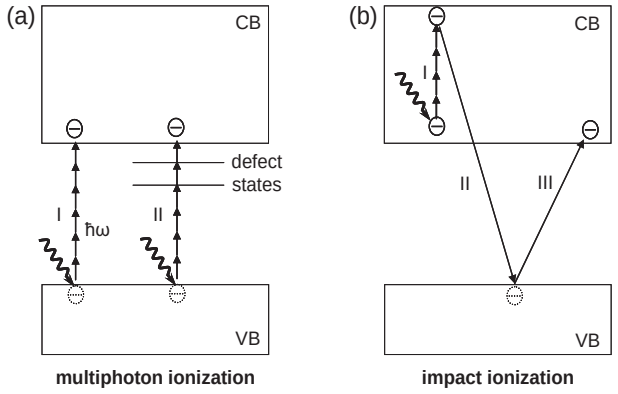

Fig. 1.3: Ionization mechanisms in wide band-gap dielectrics: (a) multiphoton absorption across the band gap (I) and resonance enhancement by defect states (II); (b) impact ionization: a conduction band electron gains additional energy in the laser field via inverse Bremsstrahlung (I), after that it transfers its kinetic energy to a valence band electron (II), thus exciting it to the conduction band (III).

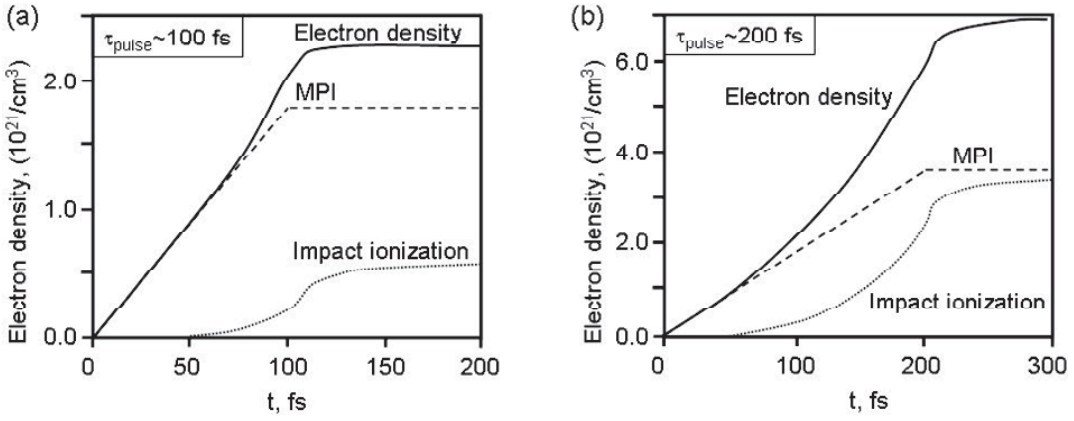

Fig. 1.4: Temporal dynamics of free electron density in the conduction band of an insulator irradiated with a laser pulse of (a) 100 fs and (b) 200 fs duration (E_{laser}=150 MV/cm). The total free electron density (solid line) is a sum of electron density produced by multiphoton ionization only (dashed line) and by impact ionization (dotted line) [KRV00]).

Considering microscopic interaction mechanisms of ultrashort laser irradiation with dielectrics and taking into account conservation of energy and momentum, Kaiser *et. al*. calculated the contribution of different ionization processes to the laser generated free electron density [KRV00]. Numerical results for a 100 fs laser pulse are

presented in Fig. 1.4 (a): while multiphoton ionization starts immediately with the beginning of the irradiation and increases linearly during the pulse, the impact/avalanche ionization is activated much later and its contribution to the electron density is not significant in comparison to the MPI. The authors [KRV00] found that only for pulse duration $\tau_{pulse} \geq 200$ fs, the density of impact electrons may become comparable to the MPI contribution (Fig. 1.4 (b)).

1.2.2. Absorption of laser irradiation in *silicon*

When laser radiation with energy $\hbar\omega$ slightly above the bandgap width E_{gap} interacts with silicon (Si), light is absorbed by the electronic system via interband linear or nonlinear (two- or more-photon) absorption that results in the generation of electron-hole (*e*-*h*) pairs. Intraband free carrier absorption (inverse Bremsstrahlung) is also possible, but it is, mainly, a secondary process, because it depends on the number of already existing carriers. Moreover, the process becomes important for Si only for the longer laser pulses or at the shorter wavelength [PVH98].

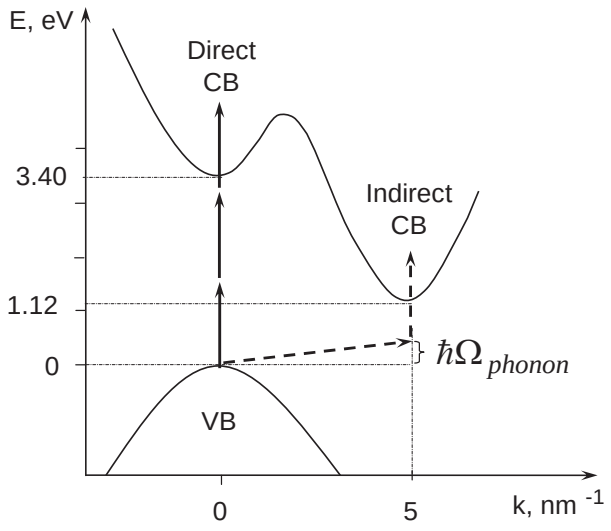

Fig. 1.5: Simplified energy diagram of electronic transitions in silicon upon irradiation with near-IR ultrashort laser pulses (E_{photon}=1.5 eV) of 100 fs duration. Direct and indirect electron transitions across the bandgap of silicon are shown with arrows.

To illustrate the possible absorption mechanisms in silicon after excitation at ~800 nm (E_{photon}=1.55 eV) with 100-fs laser pulses, the simplified energy band diagram is represented in Fig. 1.5. The energy is chosen to be zero at the edge of the valence band (VB). The direct conduction band (CB) minimum at k = 0 nm^{-1} occurs at 3.40 eV, and the indirect CB minimum (k = 5 nm^{-1}) is equal at 1.12 eV. For laser irradiation (E_{photon}=1.55 eV) at an intensity near the single-shot ablation threshold

[BBK02], the initial electronic excitation can occur through the indirect CB by one-photon absorption (dashed arrows in Fig. 1.5), which involves a phonon to satisfy momentum conservation. Along with the indirect band-band excitation, the direct transition from valence to conduction band ($E_{gap} \approx 3.40$ eV) [Sin93] is also possible by simultaneous absorption of three photons.

For a near-IR ultrashort laser pulse, it is assumed that absorption of the leading edge occurs at the depth about of $\alpha^{-1} \sim 10$ μm, where α is the optical absorption coefficient, and the rest of the pulse can be absorbed only in a shallow surface layer (0.1-0.2 μm) due to generation of a dense electron-hole (*e*-*h*) plasma at the surface region. This modeling is based on changes in optical reflectivity of a Si surface irradiated with 100-fs laser pulses at 625 nm, reported by Sokolowski-Tinten and von der Linde [SoL00]. In this work it has been shown that for a wide range of fluencies (up to 0.4 J/cm²), multiphoton absorption is the main mechanism of the electron-hole plasma formation, but also higher orders of nonlinearity are possible. Further, they estimated that the maximal density of the laser generated plasma can be over 10^{22} cm^3.

It is necessary to note here that such high concentration of *e*-*h* pairs [SoL00] can probably be expected only in the volume of the target, whereas the surface shallow layer will be considerably depleted due to appreciable emission of photoelectrons. The total electron yield in Si irradiated with 800 nm laser pulses, estimated numerically by Choi *et al.* [ChG02], can reach 10^{20} cm^{-2}. Moreover, numerous time-of-flight measurements have revealed that a substantial number of electrons instantaneously leave the surface upon femtosecond laser pulsed irradiation already at intensities well below the ablation threshold [Cos07]. These facts show that the important question concerning the real density of the fs-laser-induced plasma at the sample surface is still open.

1.2.3. Absorption of laser energy in *metals*

Generally, metals are modeled as a periodic crystal lattice of metallic ions with electrons free-moving in the self-consistent potential field that takes into account all electron-electron and electron-ion interactions [AsM76]. By irradiation of a metal with laser light, conduction electrons may absorb the laser energy through inverse Bremsstrahlung. When the absorbed energy exceeds the work function *W* of the metal, the electron can leave the surface as shown in Fig. 1.6 (a). From Fig. 1.6 (b), the work function *W* is given by

$$W = \Delta\phi - \mu, \tag{1.6}$$